Estimation of atmospheric nutrient inputs to the Atlantic Ocean from 50°N to 50°S based on large-scale field sampling: Iron and other dust-associated elements

A. R. Baker,[1] C. Adams,[1] T. G. Bell,[1,2] T. D. Jickells,[1] and L. Ganzeveld[3]

Received 18 December 2012; revised 8 May 2013; accepted 8 July 2013; published 18 August 2013.

[1] Atmospheric inputs of mineral dust supply iron and other trace metals to the remote ocean and can influence the marine carbon cycle due to iron's role as a potentially limiting micronutrient. Dust generation, transport, and deposition are highly heterogeneous, and there are very few remote marine locations where dust concentrations and chemistry (e.g., iron solubility) are routinely monitored. Here we use aerosol and rainwater samples collected during 10 large-scale research cruises to estimate the atmospheric input of iron, aluminum, and manganese to four broad regions of the Atlantic Ocean over two 3 month periods for the years 2001–2005. We estimate total inputs of these metals to our study regions to be 4.2, 17, and 0.27 Gmol in April–June and 4.9, 14, and 0.19 Gmol in September–November, respectively. Inputs were highest in regions of high rainfall (the intertropical convergence zone and South Atlantic storm track), and rainfall contributed higher proportions of total input to wetter regions. By combining input estimates for total and soluble metals for these time periods, we calculated overall percentage solubilities for each metal that account for the contributions from both wet and dry depositions and the relative contributions from different aerosol types. Calculated solubilities were in the range 2.4%–9.1% for iron, 6.1%–15% for aluminum, and 54%–73% for manganese. We discuss sources of uncertainty in our estimates and compare our results to some recent estimates of atmospheric iron input to the Atlantic.

Citation: Baker, A. R., C. Adams, T. G. Bell, T. D. Jickells, and L. Ganzeveld (2013), Estimation of atmospheric nutrient inputs to the Atlantic Ocean from 50°N to 50°S based on large-scale field sampling: Iron and other dust-associated elements, *Global Biogeochem. Cycles*, *27*, 755–767, doi:10.1002/gbc.20062.

1. Introduction

[2] The atmospheric transport of mineral dust plays a major role in the supply of nutrients such as iron (Fe) to the oceans [*Jickells et al*., 2005] and has a significant influence on the radiative balance of the atmosphere [*Prospero and Lamb*, 2003; *Chiapello et al*., 2005]. This transport is highly heterogeneous on a variety of spatial and temporal scales [*Prospero and Lamb*, 2003; *Ben-Ami et al*., 2009]. Heterogeneity makes the impacts of dust on climate (both direct radiative effects and indirect effects through the influence of nutrient deposition on oceanic carbon uptake) difficult to assess and therefore requires the use of complex computer models of dust uplift, transportation, and deposition. These models, in turn, need to be validated with sufficient appropriate observational data to ensure that they reliably reproduce the natural dust cycle [*Mahowald et al*., 2005].

[3] Remote-sensing techniques, both ground-based [*Basart et al*., 2009] and from satellite-borne sensors [*Ben-Ami et al*., 2009; *Adams et al*., 2012], are increasingly providing useful data on atmospheric dust transport, whereas long-term records of dust concentrations and chemical characteristics are provided by the measurements at dust collection sites. For estimating transport over the oceans, these dust collection sites are restricted to a few island or coastal locations. For instance, in the North Atlantic, records exist for sites at Barbados, Miami, Bermuda, Mace Head, and Izaña [*Arimoto et al*., 1995; *Prospero*, 1999; *Prospero and Lamb*, 2003; *Prospero et al*., 2010], with Barbados having by far the longest and most coherent record. In the South Atlantic, however, there are no equivalent atmospheric dust records at all.

[4] Mineral dust is the dominant atmospheric source of iron and other trace metals to the ocean. Much of the motivation for studying atmospheric dust supply to the ocean comes from the desire to better understand the role of iron inputs in the

[1]Laboratory for Global Marine and Atmospheric Chemistry, School of Environmental Sciences, University of East Anglia, Norwich, UK.
[2]Now at Plymouth Marine Laboratory, Plymouth, UK.
[3]Department of Environmental Sciences, Wageningen University and Research Centre, Wageningen, Netherlands.

Corresponding author: A. R. Baker, Laboratory for Global Marine and Atmospheric Chemistry, School of Environmental Sciences, University of East Anglia, Norwich Research Park, Norwich NR4 7TJ, UK. (alex.baker@uea.ac.uk)

0886-6236/13/10.1002/gbc.20062

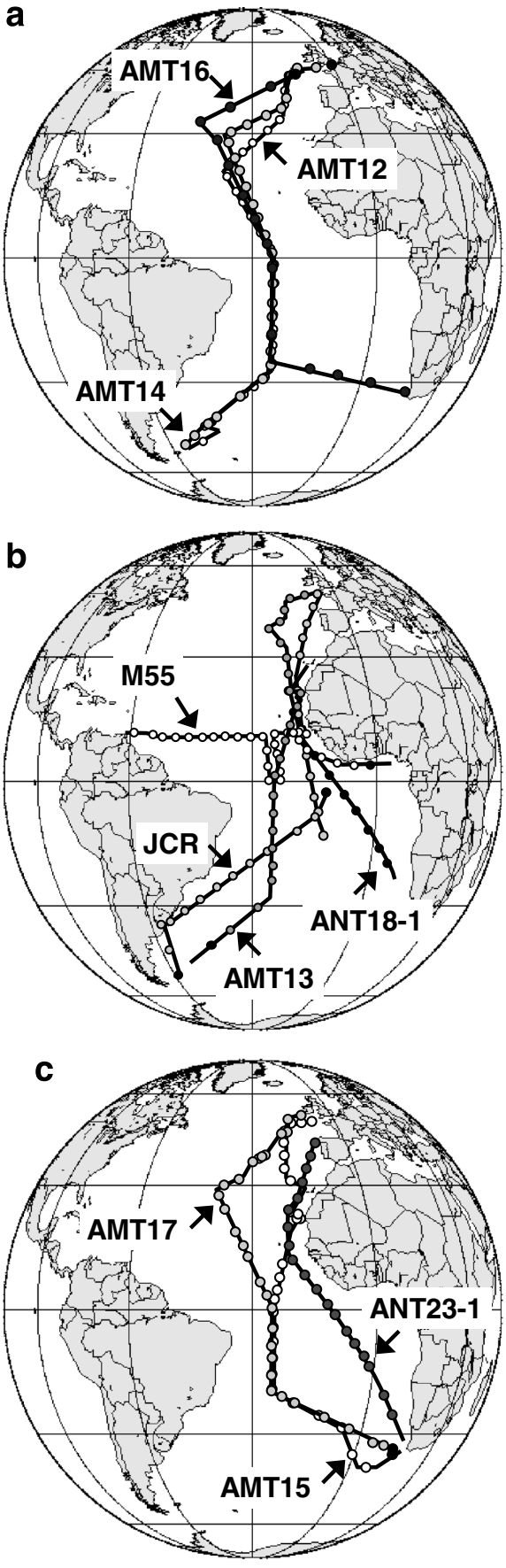

marine carbon cycle, where it is an essential nutrient for both photosynthesis and nitrogen fixation [*Boyd and Ellwood*, 2010]. It is well known that only a fraction of aerosol iron is soluble in seawater [*Jickells et al*., 2005], and it is becoming increasingly apparent that this fraction is not fixed and is likely to vary geographically [*Baker et al*., 2006c; *Fan et al*., 2006].

[5] In this work we use data obtained from aerosol and rain sampling during a series of long transect cruises to estimate atmospheric trace metal (and hence dust) fluxes to the Atlantic Ocean. We have already used similar methods to assess annual atmospheric nitrogen inputs to the Atlantic, by coupling observations of aerosol and rainfall species concentrations to air transport and rainfall climatologies [*Baker et al*., 2010]. In the present study, we use our estimates of both soluble and total iron (and aluminum and manganese) atmospheric input to produce broad-scale estimates of trace metal fractional solubility over the basin. We also discuss sources of uncertainty in our estimates and compare our results to other estimates of atmospheric dust input to the Atlantic.

2. Methods

[6] As with our earlier work on N [*Baker et al*., 2010], our estimates of atmospheric trace metal input to the Atlantic are based on aerosol and rain samples collected on a series of long transect cruises in the Atlantic over the period 2000–2005. By combining chemical data for large numbers of rain (70) and aerosol (207) samples with two separate climatologies, one of rainfall rate and the other of air mass transport, each covering the 5 years, 2001–2005, we scale up the observational database to provide flux estimates for various regions of the Atlantic.

[7] The estimates of atmospheric dust-associated element inputs presented here differ in two important respects from those of our earlier work. First, we consider that neither the total number of samples collected in the northwest Atlantic nor the geographic distribution of those samples is adequate for our purposes. We therefore only report estimates of atmospheric inputs to four of the five regions that we used in our N study and not for the northwest Atlantic. Second, unlike N transport [*Prospero et al*., 1996], mineral dust transport over the Atlantic is strongly seasonal [e.g., *Liu et al*., 2008; *Basart et al*., 2009; *Ben-Ami et al*., 2009; *Adams et al*., 2012]. We therefore confine our dust input estimate to the seasons for which we have observational data and have modified our air transport and rainfall climatologies accordingly.

2.1. Sampling and Analysis

[8] Cruise tracks and aerosol sampling start locations are shown in Figure 1. Further details of the cruises can be found in the supporting information (Table S1).

Figure 1. Locations of aerosol samples used in this work for cruises which took place in (a) April–June 2003–2005 and (b) September–November 2000–2003 and (c) September–November 2004–2005. Markers show sampling start positions. Aerosol collection generally continued until the beginning of the following sample. Sampling end positions for each cruise are shown by black markers.

[9] Sampling methods for aerosol collection, including measures taken to avoid ship-based contamination, collector flow rates, and blank collection procedures, have been described elsewhere [*Baker et al*., 2006b; *Baker et al*., 2007]. Whatman 41 collection substrates (either using Sierra-type cascade impactors with separation into coarse (>1 μm diameter) and fine (<1 μm diameter) particles, or using a single bulk filter (see Table S1)) were used during most cruises, although coarse aerosol sampling during the ANT18-1 cruise was done using quartz substrates [*Sarthou et al*., 2003]. These had rather high blanks for total metals, and consequently, we do not report total metal data for that cruise. One sample during ANT18-1 (ANT18-1/A1) was collected using six cascade impactor stages, giving fractions with modal sizes of >12.5, 5, 2.4, 1.6, 0.9, 0.4, and <0.1 μm. All aerosol collection substrates were washed with dilute acids before use in order to reduce trace metal blanks (see Table S2). Results of blank determinations and aerosol detection limits are reported in Tables S2 and S3.

[10] Rain samples were collected by manually opening rain collectors (low-density polyethylene bottles attached to 28 or 40 cm diameter polypropylene funnels) immediately prior to, or at the onset of, rain and closing them upon the cessation of rain. Rain sampling equipment was cleaned prior to use by soaking in 10% vol/vol (1.58 M) HNO_3 for at least 48 h before use, and bottles were stored, filled with acidified (15.8 mM Aristar HNO_3) ultrapure water, as described in *Baker et al*. [2007]. Blanks for rain sampling were determined during each cruise by collecting acidified (15.8 mM HNO_3) ultrapure water that had been used to rinse the collection surfaces of the rain funnels and determine the trace metal content of this rinse water (see Table S4). For three cruises (ANT18-1, JCR, and M55), subsamples of rainfall were filtered through acid-washed 47 mm 0.2 μm Sartorius cellulose acetate filters housed in acid-washed Millipore filtration rigs immediately after collection, allowing us to estimate the soluble and total metal contents of these samples. All rain samples (filtered and unfiltered) for these cruises were acidified within 3 h of collection to a final concentration of 15.8 mM with concentrated Aristar HNO_3 and frozen. For all other cruises, samples were frozen immediately without filtration and were subsequently acidified as above and left to stand for at least 2 weeks before analysis. Figure 2 shows the locations of the rain samples collected.

[11] Aerosol and rain samples were stored frozen and later thawed and analyzed using methods discussed elsewhere [*Baker et al*., 2006a; *Baker et al*., 2006c; *Baker et al*., 2007], which for the components of interest here involve graphite furnace atomic absorption spectroscopy (GFAAS) or inductively coupled plasma-optical emission spectrometry (ICP-OES) for (soluble) Fe, Al, and Mn in rain and for soluble Fe, Al, and Mn in aerosol extracts at pH 4.7 (1.1 M ammonium acetate buffer, see *Baker et al*. [2007]). For JCR and M55, total aerosol Fe, Al, and Mn were determined by GFAAS/ICP-OES after digestion with concentrated HF/HNO_3, as described by *Baker et al*. [2006c]. For the other cruises, total aerosol metals were determined by instrumental neutron activation analysis (INAA) at the Ecole Polytechnique, Montreal's SLOWPOKE nuclear reactor at a neutron flux of 5×10^{11} cm^2 s^{-1}. The samples (fractions of bulk or all size fractions of segregated samples combined) were introduced in the reactor, packed in a plastic bag, rolled into 7 mL polyethylene irradiation vials. After activation, the emission of gamma radiation at energies of 1099 (Fe-59), 1779 (Al-28), and 847 keV (Mn-55) was detected and the amount of iron, aluminum, or manganese was calculated by comparing with emissions from the standard solutions of each element. A subset of the samples that had been analyzed by the strong acid digestion method was also analyzed by INAA. This intercomparison indicated no significant differences between the two methods for Fe, Al, and Mn (paired *t* test, all $p < 0.05$, $n = 11$).

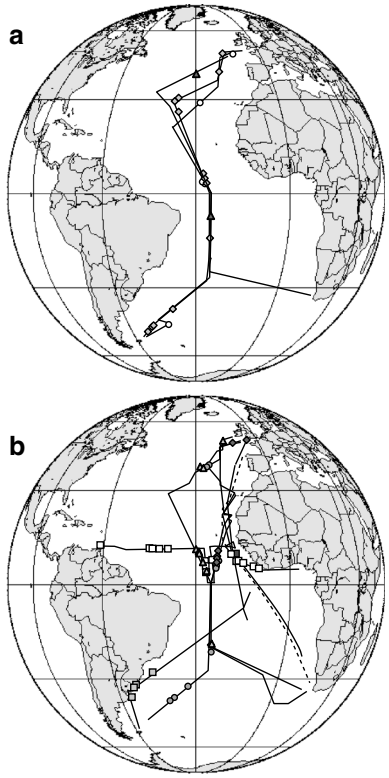

Figure 2. Locations of rainfall samples collected during this work for cruises which took place in (a) April–June and (b) September–November. Shapes indicate cruises which took place in 2000–2002 (squares), 2003 (circles), 2004 (diamonds), and 2005 (triangles), with solid symbols corresponding to those used for aerosol sampling locations in Figure 1. Rainfall was not collected during cruise ANT23-1 (dashed line).

2.2. Wet and Dry Deposition Climatologies

[12] Here we give a brief summary of the methods used to compile rainfall rate and air mass history climatologies, and specify differences to the climatologies used in our earlier study on N deposition [*Baker et al*., 2010]. Full details of the methods used can be found in *Baker et al*. [2010]. The principal difference to our earlier work is that here we treat only the 6 months of the year for which we have observational data in constructing the climatologies. As mentioned above, we do not report atmospheric input estimates for the northwest Atlantic here, although we do give whatever information we have for that region where possible.

[13] For the wet deposition climatology, we calculated average precipitation rates for the two "seasons" April–June (AMJ) and September–November (SON) for which we have rainwater concentration data. Precipitation rates were obtained from the $2.5 \times 2.5°$ gridded monthly output of the CMAP model updated from *Xie and Arkin* [1997] (http://www.cdc.noaa.gov/cdc/data.cmap.html). Using that data, we calculated average precipitation rates (P) for five broad regions having relatively high (intertropical convergence zone (ITCZ; R3) and North and South Atlantic storm tracks (R1 and R5)) and low (North and South Atlantic dry regions (R2 and R4)) rainfall (Figure 3). Average precipitation rates varied from $0.6\,\mathrm{mm\,d^{-1}}$ in Region 4 in SON to $4.9\,\mathrm{mm\,d^{-1}}$ in Region 3 in AMJ. For each of those regions, we calculated volume-weighted-mean (VWM) rainfall trace metal concentrations from the compositions of the individual rain samples (equation (1)) and then wet deposition flux (equation (2)) for each species in the AMJ and SON periods.

$$C_R = \frac{\sum C_i V_i}{\sum V_i} \tag{1}$$

where C_i is the measured concentration and V_i the volume of rain collected for each sample. The use of individual sample volumes here introduces some uncertainty into this calculation, because quantitative recovery of precipitation is very difficult aboard ship, generally being underestimated. The impact of this under-sampling on measured and calculated concentrations (C_i and C_R) is not easily estimated because concentration typically varies with the duration of the precipitation event.

$$F^w = C_R P \tag{2}$$

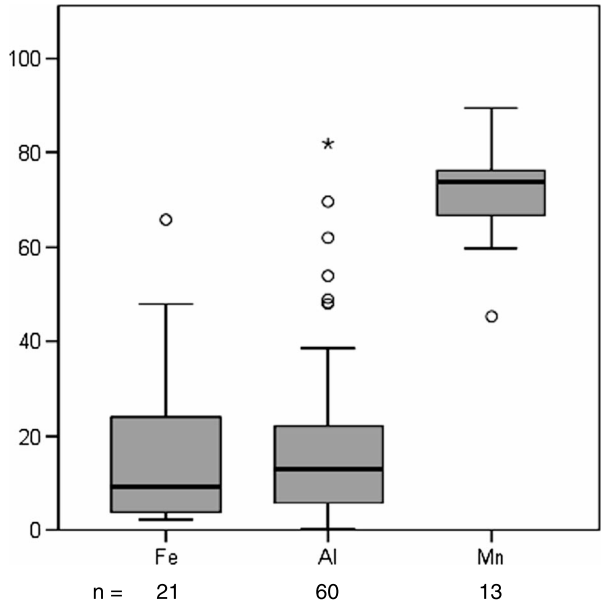

Figure 4. Box and whisker plots showing the percentage of soluble Fe, Al, and Mn in rain samples collected over the Atlantic Ocean. Also shown is the number of observations (n) in each category. Outliers more than 1.5 times the interquartile range are indicated by circles and extremes greater than three times the interquartile range by stars.

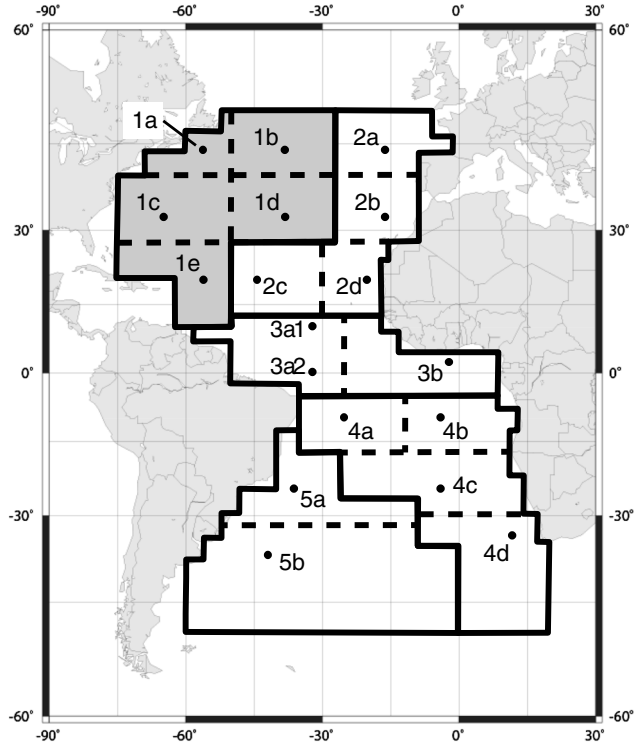

Figure 3. Map showing the boundaries (solid lines) of the deposition regions used in this study. Labels (2a–5b) identify dry deposition subregions (dashed lines), with points showing locations at which air mass back trajectories were obtained for the determination of the air mass climatology.

[14] For the calculation of soluble trace metal wet deposition fluxes, we did not have filtered rain samples for many of the cruises (see above). In those cases, we estimated soluble trace metal concentrations from total concentrations using median values for the fraction of total concentration that passed through a 0.2 or 0.45 μm filter, using our own data (Fe data from *Sarthou et al*. [2003] and *Baker et al*. [2007], and unpublished Al and Mn data for the same samples) and values reported by *Prospero et al*. [1987], *Lim et al*. [1994] (for Al), and *Buck et al*. [2010] (for Fe and Al). These data are summarized in Figure 4. This operational definition of soluble trace metal fraction will inevitably include a contribution from colloidal, as well as truly dissolved, material.

[15] Our dry deposition climatology is based on the observation that for many species, aerosol concentrations over the ocean are related to the source regions that an air mass has had contact with in the recent past [e.g., *Baker et al*., 2006b]. Here we use the same source regions as in our earlier work on nitrogen deposition [*Baker et al*., 2010], namely North America (NAmer), Europe (Eur), North Africa (Sahara), Southern Africa (SAfr), Southern Africa influenced by biomass-burning emissions (SAfr-BB), South America (SAmer), and remote air that had been circulating over the ocean (in either hemisphere) for 5 days prior to collection (NAtl-Rem and SAtl-Rem). The inclusion of a separate SAfr-BB source is justified for nitrogen because biomass

Table 1. Percentage Occurrence of Different Air Mass Types (w_i^{am}) at Selected Points in the Atlantic, Based on Analysis of Daily 5 Day Air Mass Back Trajectories for the Months of April–June (AMJ) and September–November (SON) in the Years 2001–2005

	NAmer	NAtl-Rem	Eur	Sahara	SAfr	SAfr-BB	SAtl-Rem	SAmer
AMJ								
1a	51.8	48.0	0.2					
1b	23.6	74.8	1.7					
1c	51.1	48.9						
1d	11.1	87.5	0.9	0.5				
1e	1.5	98.0		0.4				
2a	5.3	81.8	12.9					
2b	3.8	78.7	14.0	3.6				
2c	1.3	96.5	0.2	2.0				
2d	0.9	62.4	6.8	29.9				
3a1		61.2	0.7	37.9			0.2	
3a2		10.1		2.3	52.4	13.3	21.8	
3b		0.4			58.2	11.9	29.5	
4a					90.8	8.4	0.9	
4b					40.4	40.9	18.7	
4c					17.6	4.9	76.8	0.7
4d					3.8	1.3	93.3	1.6
5a						5.7	77.9	16.4
5b						1.1	48.5	50.3
SON								
1a	51.6	48.4						
1b	31.2	65.2	3.3	0.2				
1c	50.9	49.1						
1d	11.3	84.6	2.9	1.1				
1e	3.1	95.3		1.6				
2a	10.3	71.8	17.5	0.5				
2b	4.0	68.7	19.3	8.0				
2c	0.4	87.9	0.4	11.3				
2d	0.2	28.4	5.3	65.9			0.2	
3a1		48.9		42.7			8.4	
3a2					47.3	48.6	6.1	
3b				5.3	34.8	2.2	57.6	
4a					73.4	25.3	1.3	
4b					47.9	20.7	31.4	
4c					9.3	4.9	85.6	0.2
4d					2.0	0.9	95.3	1.8
5a						12.7	76.4	10.9
5b						3.9	55.5	40.6

burning is a significant source of both reduced and oxidized nitrogen [*Andreae and Merlet*, 2001]. We include this source specifically here because biomass burning has been suggested to be a potentially significant source of soluble Fe [*Guieu et al*., 2005; *Luo et al*., 2008]. Samples influenced by biomass burning were identified using nonseasalt potassium as a tracer [*Baker et al*., 2006b; *Baker et al*., 2010]. In order to assess the contribution of each source region to air flow over the Atlantic, we subdivided the wet deposition regions discussed above into smaller subregions (Figure 3). We then obtained 5 day air mass back trajectories for points within each subregion using ECMWF archive data from the British Atmospheric Data Centre (http://badc.nerc.ac.uk/community/trajectory/) for each day of the 5 year period and classified them according to which source region they had passed over. The criteria used to make this classification were identical to those we used in our earlier work [*Baker et al*., 2010]. Table 1 shows the fractional occurrence of each air mass type (w^i) at each climatology point for the AMJ and SON periods.

[16] Aerosol samples were also classified according to the same criteria using 5 day air mass back trajectories obtained from the NOAA Hybrid Single-Particle Lagrangian Integrated Trajectory model (FNL data set). In each of the five large regions in each season, we calculated the median aerosol concentrations (C_A^i) for each air mass type and these median values were assumed to be representative of the aerosol concentrations associated with that air mass type in each region. Dry deposition fluxes were then calculated from these concentrations using aerosol particle size- and wind speed-dependent dry deposition velocities (v_d) for fine and coarse aerosols, as described in *Baker et al*. [2010]. We calculated dry deposition velocities for each subregion and time period using the method of *Ganzeveld et al*. [1998], utilizing climatological mean wind speeds for the relevant months of 2001–2005 obtained from the ECMWF ERA-Interim data set and particle sizes of 0.6 μm for submicron particles and 5 μm for supermicron particles. These values were derived from mass median diameters calculated for soluble Fe for the seven size fractions of sample ANT18-1/A1 (see above). The calculated deposition velocities fall in the range 0.02–0.03 and 0.4–1.1 cm s^{-1} for fine and coarse modes, respectively. Each air mass' contribution to the total deposition in each subregion was weighted according to its fractional contribution to the total air flow there (w^i, Table 1), as derived from the air mass classification scheme (equation (3)):

$$F^{d,\,int} = \sum w^i \left(C_A^{c,i} v_d^c + C_A^{f,i} v_d^f \right) \quad (3)$$

[17] For the AMT16 and ANT23-1 cruises for soluble metals and for most cruises for total metals, we only collected bulk (i.e., non-size fractionated) aerosol concentrations. In those cases, we artificially split these values into fine and coarse components using median fractions of each species occurring in the coarse mode derived from our size-fractionated data (see Table S5) as done previously [*Baker et al*., 2010].

3. Results

[18] Below we summarize atmospheric trace metal concentrations and deposition fluxes obtained in our study.

3.1. Wet Deposition—Rainfall Chemical Characteristics and Deposition Fluxes

[19] In Table 2, we show concentrations of total rainwater Fe, Al, and Mn for each deposition region in the AMJ and

Table 2. Concentration Ranges (nmol L^{-1}) and Number of Samples (in Parentheses) for Total Fe, Al, and Mn, and Their Volume-Weighted-Mean Concentrations (C_R) for the Rain Samples Collected in Each of the Wet Deposition Regions During the Periods April–June (AMJ) and September–November (SON)

Region	Fe	C_R^{Fe}	Al	C_R^{Al}	Mn	C_R^{Mn}
AMJ						
NAtl Storm	117–534 (3)	229	86–1750 (3)	404	14–76 (3)	28
NAtl Dry	367 (1)	367	1070, 1290 (2)	1130	32, 71 (2)	42
ITCZ	20–716 (7)	213	15–1160 (7)	462	1.1–44 (7)	15
SAtl Dry	42, <176 (2)	58	118, 287 (2)	138	4.0, 18 (2)	5.6
SAtl Storm	189, 724 (2)	228	197–4290 (4)	2080	<6.4–49 (4)	31
All		204		683		19
SON						
NAtl. Storm	110–2240 (4)	680	165–4760 (4)	1470	6.2–77 (4)	28
NAtl. Dry	40–637 (5)	82	25–2160 (5)	182	0.9–60 (5)	5.9
ITCZ	33–2050 (33)	515	40–6930 (35)	1350	<0.5–153 (31)	25
SAtl Dry	35–105 (5)	70	<27–424 (5)	140	4.0–24 (5)	17
SAtl Storm	<30–1440 (5)	338	97–5420 (5)	701	2.6–28.3 (5)	10
All		493		1250		23

Table 3. Examples of Previously Reported Concentrations (nmol L^{-1}) and Number of Observations (Where Available) for Total Iron, Aluminum, and Manganese in Rainfall Samples in Each of the Five Deposition Regions Used in This Work

Region	Month	Fe	Al	Mn	*n*	References[a]
1	Aug	314[b]			12	A
1	Mar	225[b]			4	A
2[c]		0.9–495	4.8–431	0.5–7.3	12	B
2[c]	Jun	25.6	103		1	C
3	Oct/Nov	150–1140	330–4860	8.3–62	3	D
3	Jun	54–3300 (680[b])		1.6–160 (31.0[b])	17	E
3	Jul	132–419	414–1404		4	C
4	May/Jun	3.6, 16			2	E
5	Nov	30, 62	48, 380	2.0, 3.8	2	D
5	May	121		2.0	1	E

[a]References: A, *Kieber et al*. [2003]; B, *Lim et al*. [1991]; C, *Buck et al*. [2010]; D, *Helmers and Schrems* [1995]; E, *Kim and Church* [2002].
[b]Volume-weighted-mean concentration.
[c]North of Region 2.

SON seasons, and volume-weighted-mean concentrations for each region and for the Atlantic as a whole in each season. Overall, the concentrations of rainwater trace metals ranged from 20 to 2240, 15–6930, and <0.5–153 nmol L^{-1} for Fe, Al, and Mn, respectively. VWM concentrations for each species were higher in SON than in AMJ (e.g., for Fe, the VWM concentrations for all samples were 204 nmol L^{-1} in AMJ and 493 nmol L^{-1} in SON), although some caution may be necessary in interpreting this difference because of the low number of samples available for AMJ (~15, compared to ~50 in SON). Our data are in reasonable agreement with previously published rainwater trace metal concentrations (Table 3), although in several of our deposition regions, and for Mn in general, there is very little other data available.

[20] In Table 4, we show our calculated wet deposition fluxes for total metals in Regions 2–5. Fluxes were lowest in Region 4 for all metals, as a result of low rainfall concentrations and precipitation rates, and highest in Region 3, where both concentrations and precipitation were high. As stated above, we used median values of percentage of soluble rainwater trace metals (9.4%, 13%, and 74% for Fe, Al, and Mn, respectively) to calculate soluble metal concentrations for most of our rain samples. Soluble metal wet deposition fluxes (Table 4) were of similar percentages with their respective total wet fluxes, since most of the soluble metal data were calculated in this way, rather than measured directly.

Table 4. Precipitation Rate (*P*, mm d^{-1}) and Wet Deposition Fluxes (nmol m^{-2} d^{-1}) of Soluble and Total Fe, Al, and Mn to Deposition Regions for the Periods April–June (AMJ) and September–November (SON)

Region	*P*	Sol Fe	Sol Al	Sol Mn	Tot Fe	Tot Al	Tot Mn
AMJ							
1	2.7	-	-	-	-	-	-
2	0.7	24.6	104	22.2	260	800	30
3	4.9	97.4	292	52.1	1040	2250	71
4	1.0	5.4	17.7	4.1	58	140	5.5
5	3.5	74.2	937	80.5	790	7210	110
SON							
1	3.8	-	-	-	-	-	-
2	2.2	16.8	51.3	9.4	180	390	13
3	4.2	114	612	66.2	2180	5690	110
4	0.6	3.9	10.7	7.3	41	82	9.9
5	3.3	231	393	27.3	1100	2300	34

3.2. Dry Deposition—Chemical Characteristics of Air Mass Types and Deposition Fluxes

[21] In Tables 5 and 6, we show median aerosol trace metal concentrations for each air mass type observed in each of the five deposition regions during the AMJ and SON periods, respectively. We also present the variation in aerosol trace metal concentrations between air mass types (without dividing the data set according to deposition region) for these two periods in Figure 5.

[22] Trace metal concentrations were generally higher in Regions 1–3 than in Regions 4 and 5, consistent with the distributions of their terrestrial sources between the hemispheres. As might be expected, aerosol trace metal concentrations were very much higher in Saharan air masses than in any other air mass type. For the total metals, no air mass type had a median concentration greater than 10% of its respective median concentration in Saharan air. For the soluble metals, however, the median concentrations of the non-Saharan air masses were of higher proportions than the

Table 5. Median Concentrations (pmol m^{-3}) and Number of Observations (*n*) for Soluble and Total Metals for the Aerosol Samples Collected During the Period April–June (AMJ) Divided According to Air Mass Type in Each of the Five Deposition Regions

Region	Air Mass	Sol Fe	Sol Al	Sol Mn	n_{Sol}	Tot Fe	Tot Al	Tot Mn	n_{Tot}
1	NAmer	-	-	-		-	-	-	
	NAtl-Rem	41.6	248	7.9	5	1210	1590	15.8	5
	Eur	-	-	-		-	-	-	
	Sahara	-	-	-		-	-	-	
2	NAmer	-	-	-		-	-	-	
	NAtl-Rem	33.5	132	9.1	14	1260	1850	19.6	14
	Eur	58.9	286	15.2	3	1280	3070	30.9	3
	Sahara	-	-	-		-	-	-	
3	NAtl-Rem	77.3	717	32.0	3	3420	10,800	56.4	3
	Eur	-	-	-		-	-	-	
	Sahara	88.9	552	45.1	4	6820	24,300	139	4
	SAfr	8.8	58.4	4.2	2	1700	6350	38.3	2
	SAfr-BB	-	-	-		-	-	-	
	SAtl-Rem	34.4	228	11.0	1	1460	4220	27.3	1
4	SAfr	24.4	94.2	5.9	2	1580	1880	16.4	2
	SAfr-BB	-	-	-		-	-	-	
	SAtl-Rem	10.7	58.4	1.9	11	363	523	7.0	11
	SAmer	-	-	-		-	-	-	
5	SAfr-BB	-	-	-		-	-	-	
	SAtl-Rem	4.6	70.9	1.5	5	379	729	4.6	5
	SAmer	4.1	32.1	0.6	3	565	788	2.6	3

Table 6. Median Concentrations (pmol m^{-3}) and Number of Observations (n) for Soluble and Total Metals for the Aerosol Samples Collected During the Period September–November (SON) Divided According to Air Mass Type in Each of the Five Deposition Regions

Region	Air Mass	Sol Fe	Sol Al	Sol Mn	n_{Sol}	Tot Fe	Tot Al	Tot Mn	n_{Tot}
1	NAmer	-	-	-		-	-	-	
	NAtl-Rem	17.4	227	2.0	6	384	534	2.0	6
	Eur	-	-	-		-	-	-	
	Sahara	-	-	-		-	-	-	
2	NAmer	-	-	-		-	-	-	
	NAtl-Rem	11.2	90.0	3.2	28	349	594	6.5	28
	Eur	61.7	367	4.5	4	240	1220	7.8	4
	Sahara	158	1820	115	17	11,500	36,700	167	15
	SAtl-Rem	-	-	-		-	-	-	
3	NAtl-Rem	82.2	702	53.4	6	5290	21,500	93.2	5
	Sahara	229	2050	159	14	19,200	79,000	341	14
	SAfr	40.3	273	18.5	22	864	2630	17.4	20
	SAfr-BB	37.7	142	9.0	8	730	1940	17.8	7
	SAtl-Rem	-	-	-		-	-	-	
4	SAfr	13.5	48.5	5.2	3	198	1120	11.8	2
	SAfr-BB	19.7	137	9.0	13	515	1520	15.7	11
	SAtl-Rem	6.4	56.5	1.5	20	376	491	3.5	20
	SAmer	-	-	-		-	-	-	
5	SAfr-BB	-	-	-		-	-	-	
	SAtl-Rem	19.2	84.3	4.0	8	167	458	8.7	8
	SAmer	25.1	350	12.7	3	222	1410	15.1	3

Saharan median concentrations (e.g., up to 37% (Eur), 19% (Eur), and 11% (SAfr) for soluble Fe, Al, and Mn respectively). A few samples in the NAtl-Rem classification had high trace metal concentrations (Figure 5). The color of these samples, which were generally located in the west of Region 3, indicated that they contained significant amounts of Saharan dust, although their air mass back trajectories did not show contact with land over the 5 days before collection.

[23] Figure 5 appears to show that trace metal concentrations in Saharan air were both higher and more variable in SON than in AMJ. This may not actually be the case. The former is probably the result of the AMJ cruises all passing through the central Atlantic, while several of the SON cruises approached much closer to the West African coast (Figure 1) and hence encountered higher dust concentrations. The apparent lower variability of AMJ concentrations may also be partly due to the uniformity of the AMJ cruise tracks through the tropical North Atlantic and may also simply be a result of the lower number of samples collected over that period (four in AMJ, 31 in SON).

[24] Our median trace metal concentration data (Tables 5 and 6) and their ranges (Figure 5) are consistent with previous ship-board studies in the Atlantic, although there is a high degree of variability in observed trace metal concentrations in all of these data. For example, total and soluble Fe concentrations have been reported in the range 1.4–134,000 pmol m^{-3} [*Völkening and Heumann*, 1990; *Losno et al*., 1992; *Rädlein and Heumann*, 1992, 1995; *Johansen et al*., 2000; *Chen and Siefert*, 2004; *Baker et al*., 2006c; *Buck et al*., 2010] and <2.0–775 pmol m^{-3} [*Johansen et al*., 2000; *Chen and Siefert*, 2004; *Baker et al*., 2006c; *Buck et al*., 2010], respectively. In Tables S6 and S7, we list examples of, respectively, total and soluble aerosol trace metal concentrations previously reported for our five deposition regions. While we have not attempted to select for data in these periods, it would appear that most previous studies have taken place in the same seasons as ours.

[25] Similarly to wet deposition, dry deposition fluxes were generally low in Region 4 in both seasons (Table 7), although the lowest dry deposition fluxes (for all species except total Fe and total Al) were recorded in Region 5 in AMJ. The highest dry deposition fluxes in both seasons occurred in Region 3 for total metals and Region 2 for soluble metals.

3.3. Total Trace Metal Inputs and Climatological Mean Solubility

[26] In Table 8, we show the total combined wet and dry inputs of trace metals to the deposition regions over each of the 3 month periods considered. For each trace metal species, inputs were lowest in Region 4 in both seasons and inputs to the high-precipitation regions (3 and 5) were generally higher than those in Regions 2 and 4 by factors of at least 2. In the high-precipitation regions, wet deposition constituted a higher proportion of the total input than in the drier regions (Figure 6 and Table S12). In almost all cases, the proportion of soluble trace metals delivered via rainfall was higher than the equivalent proportion of total trace metals (Figure 6), because the fractional solubility of rainwater trace metals is higher than their fractional solubility in aerosol.

[27] We used the inputs of soluble and total Fe, Al, and Mn presented in Table 8 to calculate overall climatological mean solubilities for each metal (% solubility = 100 × soluble input / total input). The results of these calculations are given in Table 9 and lie in the range 2.4%–20%, 6.1%–18%, and 54%–78% for Fe, Al, and Mn respectively.

4. Discussion

4.1. Sources of Uncertainty in Our Flux Estimates

[28] There are many potential sources of uncertainty in the trace metal flux estimates that we present here. Some of these uncertainties are common to our earlier estimate of nitrogen

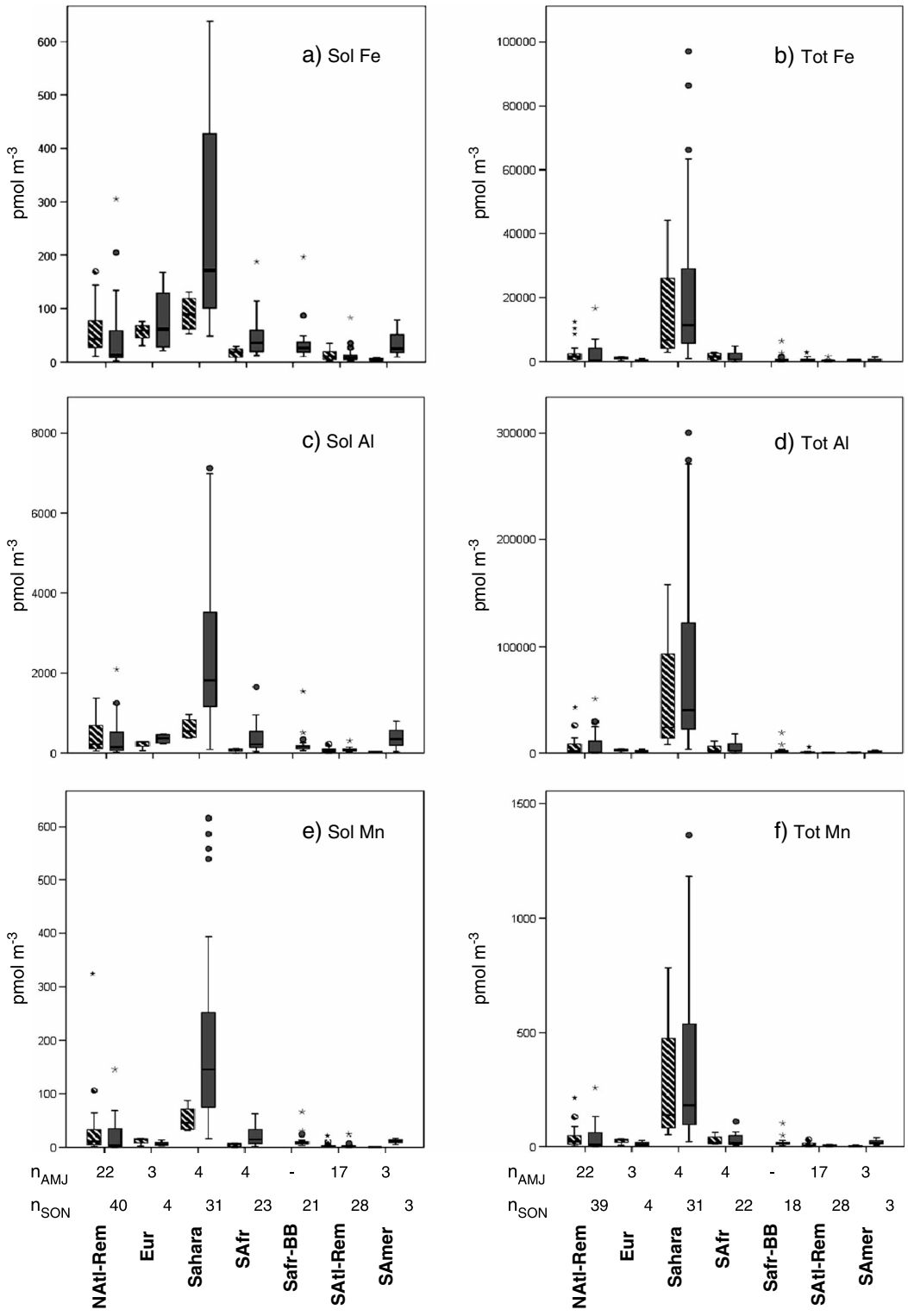

Figure 5. Box and whisker plots showing total (coarse + fine) concentrations of (a) soluble and (b) total Fe, (c) soluble and (d) total Al, (e) soluble and (f) total Mn according to air mass type for the periods April–June (hatched boxes) and September–November (grey boxes). Figures 5a–5f show the number of observations (*n*) in each category. Air mass types are defined in the text. Outliers and extremes are indicated as in Figure 4.

Table 7. Dry Deposition Fluxes (nmol m^{-2} d^{-1}) of Soluble and Total Metals to Deposition Regions for the Periods April–June (AMJ) and September–November (SON)

Region	Sol Fe	Sol Al	Sol Mn	Tot Fe	Tot Al	Tot Mn
AMJ						
1	-	-	-	-	-	-
2	10.1	58.0	4.9	561	1390	10.7
3	7.2	57.4	5.2	676	2420	14.6
4	4.0	20.2	1.3	328	421	4.4
5	1.8	15.7	0.3	218	388	1.9
SON						
1	-	-	-	-	-	-
2	11.0	133	8.9	824	2650	13.3
3	10.8	98.0	10.3	946	3750	18.8
4	2.2	19.3	1.5	101	270	3.0
5	7.3	93.1	3.7	101	454	5.8

deposition to the Atlantic and were discussed in detail there [*Baker et al*., 2010]. We identify those uncertainties below but only give specific analysis of the uncertainties peculiar to the trace metal estimate here. Where sources of uncertainty are common to the various trace metal estimates, we illustrate their impact, taking Fe as an example and only list uncertainties for metals individually where those uncertainties are metal specific, e.g., for wet inputs of soluble trace metals.

4.1.1. Wet and Dry Deposition Flux Parameterizations

[29] Rainfall rates are uncertain due to difficulties of making reliable measurements over the ocean, but this probably is not a large contributor on the broad spatial scales considered in this work [*Baker et al*., 2010].

[30] Dry deposition velocity (v_d) remains a major uncertainty in estimating atmospheric fluxes to the ocean. *Duce et al*. [1991] used a v_d value of 0.4 cm s^{-1} for bulk aerosol to estimate the dry deposition of mineral dust to the oceans. They also suggested that v_d values of 0.01 and 1 cm s^{-1} might be appropriate for fine mode (<1 μm) and mineral dust aerosols, respectively. Using these v_d values in our deposition estimate, we calculate the cumulative dry input of total Fe to Regions 2–5 in SON to be 2.3 Gmol ($v_d = 0.4$ cm s^{-1}) and 3.8 Gmol ($v_d = 0.01$ and 1 cm s^{-1}), compared to the value of 1.9 Gmol derived using the variable deposition velocities of our baseline calculation. While there is a factor of 2 difference between these deposition estimates, this is well within the uncertainty in dry deposition velocity (plus or minus a factor of 2–3) quoted by *Duce et al*. [1991] and associated with uncertainties on the role of, for example, the impact of spray formation and hygroscopic growth on aerosol deposition [*Ganzeveld et al*., 1998; *Petroff and Zhang*, 2010]. As an indication of the potential impact of this uncertainty, increasing dry deposition velocities by a factor of three increases the (dry plus wet) input of total Fe, Al, and Mn to Regions 2–5 combined by 69%, 89%, and 40%, respectively in SON.

4.1.2. Volume-Weighted-Mean Rainwater Concentrations

[31] Our wet deposition estimates are based on the assumption that the volume-weighted-mean species concentrations used in the calculations are actually representative of the rainfall in each region. Two factors are likely to affect the validity of this assumption: (i) whether the number of samples we collected was sufficient to characterize rainwater composition in each region and (ii) whether the geographic distribution of those samples was representative of the region. In the former case, we do not have sufficient other data to compare against rainwater trace metals, so we use our previous estimates for N to assess likely uncertainties. Thus, we assign uncertainties of ±20% in VWM concentrations in Region 3 in SON (for which we had more than 30 samples) and ±40% for all other regions (where we had fewer than 10 samples). This implies an overall uncertainty in our estimate of total wet input to Regions 2–5 of ±40% in AMJ and ±27% in SON. In the latter case, the distribution of our rain samples is poor in all regions (except perhaps Region 3 in SON) due to the constraints of the cruise tracks used in this study (Figure 2). We are not able to quantify the uncertainty associated with this poor sample distribution without further information on rainwater trace metal concentrations over the Atlantic. This may be a significant effect where relatively large mineral dust inputs occur (e.g., for the Sahara in Regions 2 and 3 and the Namib desert in Region 4), since these are likely to be strongest at the margins of our regions.

[32] *Ridame and Guieu* [2002] noted that very small (i.e., only a few drops) rainfall events can contribute significant amounts of dust to the western Mediterranean. Events of this type are rather difficult to sample, particularly from ships, and if a similar situation exists in the eastern North Atlantic (Region 2), our sampling would be unlikely to record them.

[33] The soluble metal wet deposition flux estimates given in Table 4 are subject to further uncertainty because of the way in which we have estimated trace metal soluble fractions in samples for which we had no soluble metal measurements. Fractional Fe and Al solubility in rainfall varies as a function of pH [*Prospero et al*., 1987; *Theodosi et al*., 2010a] and total metal load [*Theodosi et al*., 2010a]. Since we do not have rainwater pH data available and are not able to estimate metal loadings as part of our calculations, we estimate the uncertainty in soluble trace metal wet deposition fluxes using the interquartile ranges of the fractional solubility data presented in Figure 4. This approach yields ranges of wet soluble inputs of 0.33–0.63, 0.8–1.5, and 0.109–0.116 Gmol for Fe, Al, and Mn respectively in SON, compared to our baseline estimates for these species of 0.41 Gmol (Sol Fe), 1.1 Gmol (Sol Al), and 0.115 Gmol (Sol Mn).

4.1.3. Median Aerosol Concentrations

[34] As for N [*Baker et al*., 2010], we estimate the uncertainty due to poor characterization of representative aerosol

Table 8. Total (Wet + Dry) Inputs (Gmol) of Soluble and Total Fe, Al, and Mn to Deposition Regions for the Periods April–June (AMJ) and September–November (SON)

Region	Sol Fe	Sol Al	Sol Mn	Tot Fe	Tot Al	Tot Mn
AMJ						
1	-	-	-	-	-	-
2	0.032	0.15	0.025	0.76	2.01	0.037
3	0.097	0.33	0.053	1.60	4.35	0.079
4	0.014	0.056	0.008	0.57	0.82	0.015
5	0.093	1.17	0.010	1.24	9.34	0.136
SON						
1	-	-	-	-	-	-
2	0.025	0.17	0.017	0.92	2.79	0.024
3	0.116	0.66	0.071	2.91	8.79	0.116
4	0.009	0.044	0.013	0.21	0.52	0.019
5	0.290	0.60	0.038	1.48	3.37	0.049

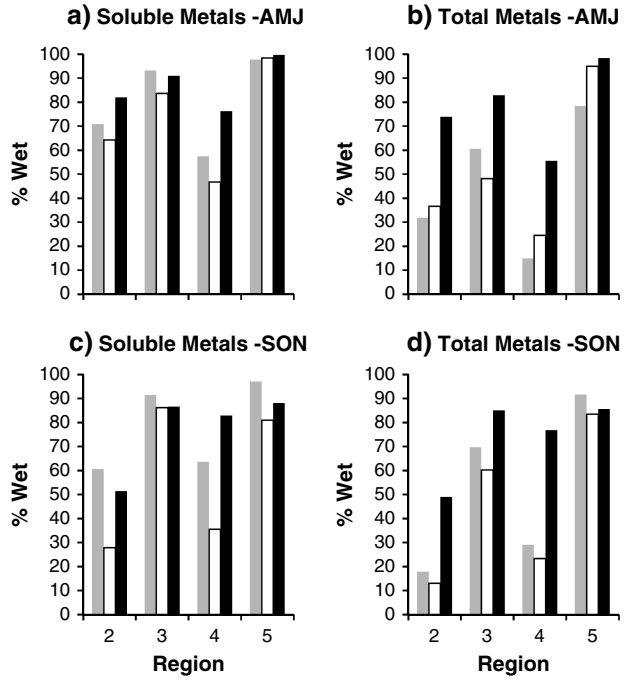

Figure 6. The percentage of total inputs to the deposition regions due to wet deposition for (a) soluble metals in AMJ, (b) total metals in AMJ, (c) soluble metals in SON, and (d) total metals in SON. Fe (grey bars), Al (white bars), and Mn (black bars).

concentrations, based on the number of samples (n) used to calculate the median concentrations for each air mass type. Thus, we assigned uncertainties of ±100%, where n was ≤2, ±50% for $3 < n \leq 5$, ±30% for $6 < n \leq 10$, and ±15% for $n > 10$. This resulted in uncertainties in dry input to the individual regions of 27%–70% in AMJ and 19%–39% in SON for soluble Fe, and 31%–86% (AMJ) and 15%–36% (SON) for total Fe. Overall uncertainties for dry inputs to Regions 2–5 combined were 50% (AMJ) and 25% (SON) for soluble Fe, and 60% (AMJ) and 21% (SON) for total Fe. As was the case for wet inputs, the geographic distribution of aerosol samples through each region is likely to affect our calculated median trace metal concentrations. We are not able to quantify the impact of this effect.

4.1.4. Wet and Dry Soluble Metal Inputs

[35] We have used somewhat different operational definitions to define the soluble fractions of the rainfall and aerosol samples in this study. In both cases, we filtered samples through 0.2 μm filters, which will lead to our "soluble" fractions containing trace metals that would more accurately be defined as "dissolved and colloidal". The pH of the rain and aerosol systems was also different. We buffered the aerosol extraction experiments at pH 4.7 but made no attempt to buffer the rain samples at a fixed value before filtration, nor did we measure the pH of any but a handful of the rain samples. Reports of rainwater pH in the remote Atlantic give values in the range 4.19–5.73 [*Losno et al*., 1991; *Lim et al*., 1994]. The samples collected in the ITCZ had higher pH values (median 5.36) than those from other regions (median 4.67), probably due to partial neutralization of acidity by $CaCO_3$ in Saharan dust in the ITCZ samples [*Loye-Pilot et al*., 1986]. Since trace metal solubility decreases with increasing pH [*Theodosi et al*., 2010a; *Theodosi et al*., 2010b], this might imply that our results overestimate the importance of dry deposition to atmospheric soluble trace metal fluxes in Region 3.

4.2. Contributions of Saharan Dust and Other Sources

[36] Our calculations allow us to assess the contributions of individual air mass types to total dry atmospheric inputs to our study region. Concentrations of soluble and total Fe, Al, and Mn were significantly higher in air masses dominated by Saharan dust than in aerosols sampled in any other air mass type (Figure 5). According to our climatological estimates for dry deposition, Saharan dust inputs to Regions 2 and 3 contribute 17% of atmospheric soluble Fe and 21% of total Fe input to Regions 2–5 in AMJ and 38% of soluble Fe and 68% of total Fe in SON. In both seasons, the contribution of Saharan dust to soluble Fe is lower than the total Fe. This is consistent with the relatively low fractional solubility of Fe in Saharan dust compared to aerosols collected from other sources reported by many workers [e.g., *Baker et al*., 2006c; *Sedwick et al*., 2007]. The percentage contribution values from Saharan dust in AMJ are surprisingly low, perhaps (as discussed above) due to the influence of the geographic distribution of the AMJ cruises on the median aerosol concentrations we used.

[37] Observations in the Mediterranean prompted *Guieu et al*. [2005] to suggest that biomass burning might be a significant source of aerosol soluble Fe to the oceans. We use our results for soluble Fe in aerosols originating from southern Africa to assess whether biomass burning might be important in the South Atlantic. The median concentration of soluble Fe in aerosol samples collected from SAfr-BB-type air masses during SON (which overlaps with the southern hemisphere biomass-burning season) was 26 pmol m^{-3} ($n = 23$) compared to 35 pmol m^{-3} ($n = 25$) in SAfr-type aerosols in the same season. These two air mass types contribute 8% (SAfr-BB) and 14% (SAfr) of the soluble Fe input to Regions 2–5 in SON according to our climatology. Thus, our results do not indicate that biomass burning is a major contributor to soluble Fe inputs to the South Atlantic.

4.3. Trace Metal Solubility

[38] Percentage solubility values (100 × soluble concentration / total concentration) for the individual aerosol samples collected during this study are in the range 0.1%–98% for

Table 9. Average Percentage Solubilities Estimated From Climatological Atmospheric Inputs of Soluble and Total Trace Metals in AMJ and SON

Region	% Fe Solubility	% Al Solubility	% Mn Solubility
AMJ			
1	-	-	-
2	4.2	7.4	67
3	6.1	7.5	67
4	2.4	6.8	54
5	7.5	12.5	73
SON			
1	-	-	-
2	2.8	6.1	70
3	4.0	7.5	61
4	4.3	8.5	68
5	20	18	78

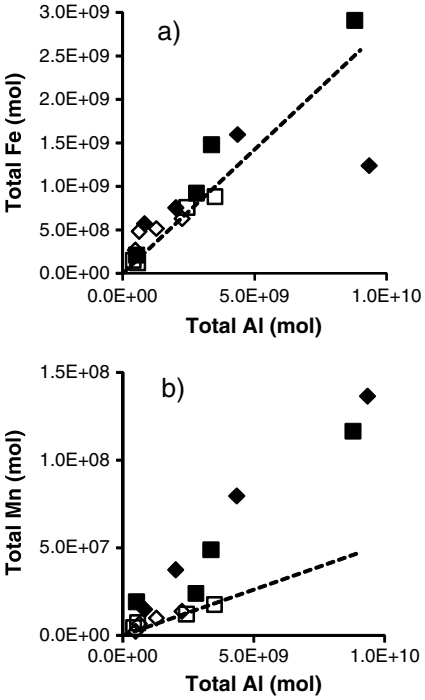

Figure 7. Inputs of (a) total Fe and (b) total Mn to our deposition regions as a function of total Al inputs. Values are shown for AMJ (diamonds) and SON (squares). Open symbols are for dry input only, and solid symbols show the sum of dry plus wet input. Also shown are the molar ratios of (Figure 7a) Fe:Al and (Figure 7b) Mn:Al for shale, taken from *Turekian and Wedepohl* [1961] (dashed lines).

Fe [*Sholkovitz et al*., 2012], 0.2%–87% for Al, and 4.5%–96% for Mn, with median values of 2.5%, 8.0%, and 50%, respectively (similar relative solubility patterns are also apparent in rainfall samples for these metals (see Figure 4 and Table 4).) For Saharan dust samples, Fe and Al solubilities lie at the lower end of these ranges (<5% and <10%, respectively), while aerosols from other air mass types had higher solubilities for these metals [*Baker et al*., 2006c]. For Fe, more soluble anthropogenic sources of Fe may contribute to the high percentage solubility of non-Saharan aerosols [*Sedwick et al*., 2007; *Sholkovitz et al*., 2012], but it is unclear whether Al solubility is also influenced by anthropogenic sources.

[39] In contrast, the percentage solubility values for Fe, Al, and Mn shown in Table 9 represent averages of the solubilities for each metal, taking into account inputs of total and soluble species in both dry and wet depositions and the cumulative contribution from all aerosol sources to each region over the 3 month periods of our study. As such, they are more representative of trace metal solubility over timescales relevant to the residence time of these species in surface seawater [*Jickells et al*., 1994; *de Jong et al*., 2007] than the measurements of solubility made on individual aerosol or rain samples. For Fe, seawater composition strongly influences the dissolution of atmospherically deposited material [*Baker and Croot*, 2010]. Therefore, in Regions 2 and 3, the actual percentage of atmospheric Fe dissolved in surface waters may be rather less than the values given in Table 9 because of the high dissolved Fe concentration of the tropical North Atlantic [*Sarthou et al*., 2003; *Measures et al*., 2008].

[40] In Figure 7, we plot our estimates of total Fe and total Mn inputs via wet plus dry (Table 8) and dry (Table S10) depositions against total Al input. Ratios of Fe:Al in dry plus wet and dry depositions and of Mn:Al in dry deposition are generally similar to the ratios of these elements in shale [*Turekian and Wedepohl*, 1961]. For Mn:Al, in wet plus dry deposition, however, there is a noticeable displacement from the shale ratio, which indicates that Mn is preferentially removed during wet deposition. We suggest that this behavior may be caused by the much higher solubility of Mn relative to Al and Fe noted above. Mn-containing (or Mn-coated) particles are likely to be more hydrophilic than Fe/Al-containing particles and therefore more likely to be incorporated into cloud droplet and subsequently rained out.

4.4. Comparison to Other Flux Estimates

[41] In Table 10, we compare our estimates of total and soluble Fe inputs to those produced by two recent modeling studies of atmospheric Fe deposition. *Mahowald et al*. [2009] estimated global total Fe inputs from modeled mineral dust deposition by assuming that Fe constitutes 3.5% of dust and soluble Fe inputs by assuming that reaction with atmospheric acids increases the solubility of hematite in dust from a baseline of 0.4% and that there is an additional source of Fe from combustion processes (4% of which is soluble). *Johnson et al*. [2010] modeled mineral dust inputs to the South Atlantic and calculated soluble Fe inputs from these, assuming 3.5% of dust is Fe and that the solubility of this Fe was determined by the uptake of acidic species on several mineral phases during atmospheric transport.

Table 10. Comparison of Soluble and Total Fe Input Estimates to our Deposition Regions (Gmol) in the AMJ and SON Periods

Species	Region	AMJ	SON
	Mahowald et al. [2009][a]		
Total Fe	2	7.07	6.34
Total Fe	3	18.4	5.46
Total Fe	4	0.91	0.75
Total Fe	5	0.52	0.91
	Johnson et al. [2010][b]		
Total Fe	4	0.16	0.23
Total Fe	5	1.91	0.75
	This work		
Total Fe	2	0.76	0.92
Total Fe	3	1.60	2.91
Total Fe	4	0.57	0.21
Total Fe	5	1.24	1.48
	Mahowald et al. [2009][a]		
Soluble Fe[c]	2	0.029	0.062
Soluble Fe[c]	3	0.125	0.127
Soluble Fe[c]	4	0.024	0.026
Soluble Fe[c]	5	0.007	0.018
	Johnson et al. [2010][b]		
Soluble Fe	4	0.001	0.001
Soluble Fe	5	0.011	0.004
	This work		
Soluble Fe	2	0.032	0.027
Soluble Fe	3	0.097	0.116
Soluble Fe	4	0.014	0.009
Soluble Fe	5	0.093	0.290

[a]N. M. Mahowald (personal communication, 2012).
[b]M. S. Johnson (personal communication, 2012).
[c]Soluble-Fe input including contribution from combustion sources of Fe.

[42] In the South Atlantic, there was a broad agreement between our estimates of total Fe input to Regions 4 and 5 and those of the two modeling studies. However, the *Mahowald et al*. [2009] estimates for Regions 2 and 3 in the North Atlantic are tenfold (in AMJ) and threefold (SON) higher than our estimates. For AMJ, this difference in Fe input estimates might be due, in part, to potential underestimation of trace metal inputs as a result of the geographic distribution of our cruises during that period (see sections 4.1.2 and 4.1.3). For SON, however, the difference is probably within the uncertainties of the two estimates. This comparison of our observational estimates with model output should be considered in the context of other model comparisons. *Huneeus et al*. [2011] found dust deposition estimates from 15 global models to agree within a factor of 10, while *Prospero et al*. [2010] reported that nine global models varied widely in their ability to reproduce the distribution and magnitude of dust deposition at sites in Florida.

[43] For soluble Fe, our input estimates are very similar to those of *Mahowald et al*. [2009] for all but Region 5, where we estimate higher soluble Fe inputs by approximately an order of magnitude. The soluble Fe input estimates of *Johnson et al*. [2010] for Regions 4 and 5 are also lower than ours by approximately an order of magnitude. The total and soluble Fe estimates from these modeling studies imply overall percentage Fe solubility values in the ranges 0.4%–3.5% [*Mahowald et al*., 2009] and 0.4%–0.6% [*Johnson et al*., 2010]. These values are generally lower than our observation-based estimates (Table 9).

[44] We also compare our results to output from a regional dust transport model [*Heinold et al*., 2011]. This model domain overlaps only with our subregions 2b and 2d (Figure 3). Our estimates of dry deposition to these regions (0.31 Gmol in AMJ and 0.59 Gmol in SON) differ by less than a factor of 2 from the modeled estimates (0.39 Gmol in AMJ and 0.35 Gmol in SON), calculated assuming dust is 3.5% Fe. We cannot directly compare our wet deposition results to the *Heinold et al*. [2011] estimate since we calculate wet inputs only for the whole of Region 2. However, the modeled wet Fe input to subregions 2b and 2d (0.92 Gmol in AMJ and 0.68 Gmol in SON) was a factor of ~4 greater than our estimates for Region 2 as a whole (0.24 Gmol in AMJ and 0.16 Gmol in SON).

5. Conclusion

[45] Using observational data from 10 research cruises, we have estimated atmospheric inputs of Fe, Al, and Mn to large regions of the Atlantic Ocean during two 3 month periods. While there are a number of uncertainties associated with our study, our total Fe input estimates are in reasonable agreement with some recent modeling studies [*Mahowald et al*., 2009; *Johnson et al*., 2010; *Heinold et al*., 2011]. Assuming that Fe is 3.5% of mineral dust mass, our estimates imply inputs of dust to the regions we examined of 6.6 Tg in AMJ and 8.8 Tg in SON. The AMJ estimate is more uncertain than that for SON due to fewer samples with poorer geographic distribution being collected in AMJ.

[46] Our soluble trace metal input estimates allow us to calculate overall trace metal solubilities for these atmospheric inputs. These solubilities take account of both wet and dry depositions and the relative contributions of aerosols from different sources, over time periods more relevant to the residence times of trace metals in surface seawater than can be achieved through analysis of individual samples. The values we obtained are generally higher than those produced by the modeling studies we compared our results to, by factors of 0.9–10 for *Mahowald et al*. [2009] and 4–37 for *Johnson et al*. [2010].

[47] This attempt to estimate the trace metal fluxes to the Atlantic would have been greatly improved by the existence of a larger, more comprehensive measurement database. The acquisition of such a database is probably beyond the scope of a single research group. Aerosol intercomparison exercises of the type currently being conducted through the international GEOTRACES program [*Morton et al*., 2013] and accessibility of atmospheric chemical data (e.g., through the Surface Ocean Lower Atmosphere Study COST 735 aerosol and rain chemistry database) will be paramount in facilitating future work in this area by providing open access to quality-assured data from many groups. The strong seasonality in mineral dust production and transport, and the restricted distribution of our cruises through the year have obliged us to confine our climatological trace metal input estimates to a seasonal basis. Achieving full annual coverage at the basin scale using the approach we have adopted will be rather difficult because few oceanographic research cruises are scheduled at high latitude during the winter months. At lower latitudes, research cruises are less subject to seasonal weather constraints and we are currently compiling an annual climatology of atmospheric nutrient and trace metal inputs to the tropical northeast Atlantic based on the methods used here [*Powell et al*., 2013].

[48] **Acknowledgments.** This study would not have been possible without the assistance and cooperation of the Masters and crews of the FS *Polarstern*, RRS *James Clark Ross*, FS *Meteor*, and RRS *Discovery*. We are also indebted to several colleagues who collected samples for us during some of the cruises reported here: K. Biswas (AMT14), M. Waeles (AMT15), S. Ussher (AMT16), T. Lesworth (AMT17), P. Croot, and C. Schlosser (ANT23-1), and to N. Mahowald, M. Johnson, and I. Tegen for providing us with their model output. Our participation in the cruises was funded by the European Union (IRONAGES project) and the UK Natural Environment Research Council (NERC). This study was supported by the NERC through the Atlantic Meridional Transect (AMT) Consortium (grant NER/O/S/2001/00680) and grants NER/B/S/2002/00301, NE/E010180/1, NE/G000239/1, and NE/F017359/1. T. Bell was supported by NERC KT grant NE/E001696/1. This is contribution 226 of the AMT program. We gratefully acknowledge the NOAA Air Resources Laboratory for the provision of the HYSPLIT transport and dispersion model and READY website (http://www.arl.noaa.gov/ready.html) used in this publication. ECMWF ERA-Interim data used in this study have been obtained from the ECMWF data server. The rainwater and aerosol chemical data used in this study are available from the COST735 marine aerosol and rain chemistry database (http://www.bodc.ac.uk/solas_integration/implementation_products/group1/aerosol_rain/). We thank two anonymous reviewers for their constructive comments on the manuscript.

References

Adams, A., J. M. Prospero, and C. Zhang (2012), CALIPSO derived three-dimensional structure of aerosol over the Atlantic and adjacent continents, *J. Clim.*, *25*, 6862–6879.

Andreae, M. O., and P. Merlet (2001), Emission of trace gases and aerosols from biomass burning, *Global Biogeochem. Cycles*, *15*, 955–966.

Arimoto, R., R. A. Duce, B. J. Ray, W. G. Jr.Ellis, J. D. Cullen, and J. T. Merrill (1995), Trace elements in the atmosphere over the North Atlantic, *J. Geophys. Res.*, *100*, 1199–1213.

Baker, A. R., M. French, and K. L. Linge (2006a), Trends in aerosol nutrient solubility along a west-east transect of the Saharan dust plume, *Geophys. Res. Lett.*, *33*, L07805, doi:10.1029/2005GL024764.

Baker, A. R., T. D. Jickells, K. F. Biswas, K. Weston, and M. French (2006b), Nutrients in atmospheric aerosol particles along the AMT transect, *Deep Sea Res. Part II*, *53*, 1706–1719.

Baker, A. R., T. D. Jickells, M. Witt, and K. L. Linge (2006c), Trends in the solubility of iron, aluminium, manganese and phosphorus in aerosol collected over the Atlantic Ocean, *Mar. Chem.*, *98*, 43–58.

Baker, A. R., K. Weston, S. D. Kelly, M. Voss, P. Streu, and J. N. Cape (2007), Dry and wet deposition of nutrients from the tropical Atlantic atmosphere: Links to primary productivity and nitrogen fixation, *Deep Sea Res. Part I*, *54*, 1704–1720.

Baker, A. R., and P. L. Croot (2010), Atmospheric and marine controls on aerosol iron solubility in seawater, *Mar. Chem.*, *120*, 4–13.

Baker, A. R., T. Lesworth, C. Adams, T. D. Jickells, and L. Ganzeveld (2010), Estimation of atmospheric nutrient inputs to the Atlantic Ocean from 50°N to 50°S based on large-scale field sampling: Fixed nitrogen and dry deposition of phosphorus, *Global Biogeochem. Cycles*, *24*, GB3006, doi:10.1029/2009GB003634.

Basart, S., C. P´erez, E. Cuevas, J. M. Baldasano, and G. P. Gobbi (2009), Aerosol characterization in Northern Africa, Northeastern Atlantic, Mediterranean Basin and Middle East from direct-sun AERONET observations, *Atmos. Chem. Phys.*, *9*, 8265–8282.

Ben-Ami, Y., I. Koren, and O. Altaratz (2009), Patterns of North African dust transport over the Atlantic: Winter vs. summer, based on CALIPSO first year data, *Atmos. Chem. Phys.*, *9*, 7867–7875.

Boyd, P. W., and M. J. Ellwood (2010), The biogeochemical cycle of iron in the ocean, *Nat. Geosci.*, *3*, 675–682.

Buck, C. S., W. M. Landing, J. A. Resing, and C. I. Measures (2010), The solubility and deposition of aerosol Fe and other trace elements in the North Atlantic Ocean: Observations from the A16N CLIVAR/CO_2 repeat hydrography section, *Mar. Chem.*, *210*, 57–70.

Chen, Y., and R. L. Siefert (2004), Seasonal and spatial distributions and dry deposition fluxes of atmospheric total and labile iron over the tropical and subtropical North Atlantic Ocean, *J. Geophys. Res.*, *109*, D09305, doi:10.1029/02003JD003958.

Chiapello, I., J. Prospero, J. Herman, and N. Hsu (2005), Understanding the long-term variability of African dust transport across the Atlantic as recorded in both Barbados surface concentrations and large-scale Total Ozone Mapping Spectrometer (TOMS) optical thickness, *J. Geophys. Res.*, *110*, D18S10, doi:10.1029/2004JD005132.

de Jong, J. T. M., M. Boyé, M. D. Gelado-Caballero, K. R. Timmermans, M. J. W. Veldhuis, R. F. Nolting, C. M. G. van den Berg, and H. J. W. de Baar (2007), Inputs of iron, manganese and aluminium to surface waters of the Northeast Atlantic Ocean and the European continental shelf waters, *Mar. Chem.*, *107*, 120–142.

Duce, R. A., et al. (1991), The atmospheric input of trace species to the world ocean, *Global Biogeochem. Cycles*, *5*, 193–259.

Fan, S. M., et al. (2006), Aeolian input of bioavailable iron to the ocean, *Geophys. Res. Lett.*, *33*, L07602, doi:10.1029/02005GL024852.

Ganzeveld, L., et al. (1998), Dry deposition parameterization of sulfur oxides in a chemistry and general circulation, *J. Geophys. Res.*, *103*, 5679–5694.

Guieu, C., et al. (2005), Biomass burning as a source of dissolved iron to the open ocean?, *Geophys. Res. Lett.*, *32*, L19608, doi:10.1029/12005GL022962.

Heinold, B., et al. (2011), Regional modelling of Saharan dust and biomass-burning smoke Part I: Model description and evaluation, *Tellus Ser. B Chem. Phys. Meteorol.*, *63*, 781–799.

Helmers, E., and O. Schrems (1995), Wet deposition of metals to the tropical North and the South Atlantic Ocean, *Atmos. Environ.*, *29*, 2475–2484.

Huneeus, N., et al. (2011), Global dust model intercomparison in AeroCom phase I, *Atmos. Chem. Phys.*, *11*, 7781–7816.

Jickells, T., et al. (1994), Atmospheric inputs of manganese and aluminum to the Sargasso Sea and their relation to surface water concentrations, *Mar. Chem.*, *46*, 283–292.

Jickells, T. D., et al. (2005), Global iron connections between desert dust, ocean biogeochemistry, and climate, *Science*, *308*, 67–71.

Johansen, A. M., et al. (2000), Chemical composition of aerosols collected over the tropical North Atlantic Ocean, *J. Geophys. Res.*, *105*, 15,277–15,312.

Johnson, M. S., et al. (2010), Modeling dust and soluble iron deposition to the South Atlantic Ocean, *J. Geophys. Res.*, *115*, D15202, doi:10.1029/12009JD013311.

Kieber, R. J., et al. (2003), Temporal variability of rainwater iron speciation at the Bermuda Atlantic Time Series Station, *J. Geophys. Res.*, *108*(C8), 3277, doi:10.1029/2001JC001031.

Kim, G., and T. M. Church (2002), Wet deposition of trace elements and radon daughter systematics in the South and equatorial Atlantic atmosphere, *Global Biogeochem. Cycles*, *16*(3), 1046, doi:10.1029/2001GB001407.

Lim, B., et al. (1991), Sequential sampling of particles, major ions and total trace metals in wet deposition, *Atmos. Environ. Part A*, *25*, 745–762.

Lim, B., et al. (1994), Solubilities of Al, Pb, Cu, and Zn in rain sampled in the marine environment over the North Atlantic ocean and Mediterranean Sea, *Global Biogeochem. Cycles*, *8*, 349–362.

Liu, D., et al. (2008), A height resolved global view of dust aerosols from the first year CALIPSO lidar measurements, *J. Geophys. Res.*, *113*, D16214, doi:10.1029/12007JD009776.

Losno, R., et al. (1991), Major ions in marine rainwater with attention to sources of alkaline and acidic species, *Atmos. Environ. Part A*, *25*, 763–770.

Losno, R., et al. (1992), Origins of atmospheric particulate matter over the North Sea and the Atlantic Ocean, *J. Atmos. Chem.*, *15*, 333–352.

Loye-Pilot, M. D., et al. (1986), Influence of Saharan dust on the rain acidity and atmospheric input to the Mediterranean, *Nature*, *321*, 427–428.

Luo, C., et al. (2008), Combustion iron distribution and deposition, *Global Biogeochem. Cycles*, *22*, GB1012, doi:10.1029/2007GB002964.

Mahowald, N. M., et al. (2005), The atmospheric global dust cycle and iron inputs to the ocean, *Global Biogeochem. Cycles*, *19*, GB4025, doi:10.1029/2004GB002402.

Mahowald, N. M., et al. (2009), Atmospheric iron deposition: Global distribution, variability, and human perturbations, *Ann. Rev. Mar. Sci.*, *1*, 245–278.

Measures, C. I., et al. (2008), High-resolution Al and Fe data from the Atlantic Ocean CLIVAR-CO2 repeat hydrography A16N transect: Extensive linkages between atmospheric dust and upper ocean geochemistry, *Global Biogeochem. Cycles*, *22*, GB1005, doi:10.1029/2007GB003042.

Morton, P., et al. (2013), Methods for sampling and analysis of marine aerosols: Results from the 2008 GEOTRACES aerosol intercalibration experiment, *Limnol. Oceanogr. Methods*, *11*, 62–78.

Petroff, A., and L. Zhang (2010), Development and validation of a size-resolved particle dry deposition scheme for application in aerosol transport models, *Geosci. Model. Dev.*, *3*, 753–769.

Powell, C. F., et al. (2013), Estimation of the atmospheric flux of iron, nitrogen and phosphate to the eastern tropical North Atlantic, in preparation.

Prospero, J. M., et al. (1987), Deposition rate of particulate and dissolved aluminum derived from Saharan dust in precipitation at Miami, Florida, *J. Geophys. Res.*, *92*, 14,723–714,731.

Prospero, J. M., et al. (1996), Atmospheric deposition of nutrients to the North Atlantic Basin, *Biogeochemistry*, *35*, 27–73.

Prospero, J. M. (1999), Long-term measurements of the transport of African mineral dust to the southeastern United States: Implications for regional air quality, *J. Geophys. Res.*, *104*, 15,917–15,927.

Prospero, J. M., and P. J. Lamb (2003), African droughts and dust transport to the Caribbean: Climate change implications, *Science*, *302*, 1024–1027.

Prospero, J. M., et al. (2010), African dust deposition to Florida: Temporal and spatial variability and comparisons to models, *J. Geophys. Res.*, *115*, D13304, doi:10.1029/2009JD012773.

Rädlein, N., and K. G. Heumann (1992), Trace analysis of heavy metals in aerosols over the Atlantic Ocean from Antarctica to Europe, *Int. J. Environ. Anal. Chem.*, *48*, 127–150.

Rädlein, N., and K. G. Heumann (1995), Size fractionated impactor sampling of aerosol particles over the Atlantic Ocean from Europe to Antarctica as a methodology for source identification of Cd, Pb, Tl, Ni, Cr, and Fe, *Fresenius J. Anal. Chem.*, *352*, 748–755.

Ridame, C., and C. Guieu (2002), Saharan input of phosphate to the oligotrophic water of the open western Mediterranean Sea, *Limnol. Oceanogr.*, *47*, 856–869.

Sarthou, G., et al. (2003), Atmospheric iron deposition and sea-surface dissolved iron concentrations in the East Atlantic, *Deep Sea Res. Part I*, *50*, 1339–1352.

Sedwick, P. N., et al. (2007), Impact of anthropogenic combustion emissions on the fractional solubility of aerosol iron: Evidence from the Sargasso Sea, *Geochem. Geophys. Geosyst.*, *8*, Q10Q06, doi:10.1029/2007GC001586.

Sholkovitz, E. R., et al. (2012), Fractional solubility of aerosol iron: Synthesis of a global-scale data set, *Geochim. Cosmochim. Acta*, *89*, 173–189.

Theodosi, C., et al. (2010a), Iron speciation, solubility and temporal variability in wet and dry deposition in the Eastern Mediterranean, *Mar. Chem.*, *120*, 100–107.

Theodosi, C., et al. (2010b), The significance of atmospheric inputs of soluble and particulate major and trace metals to the eastern Mediterranean seawater, *Mar. Chem.*, *120*, 154–163.

Turekian, K. K., and K. H. Wedepohl (1961), Distribution of the elements in some major units of the Earth's crust, *Geol. Soc. Am. J.*, *72*, 175–191.

Völkening, J., and K. G. Heumann (1990), Heavy metals in the near surface aerosol over the Atlantic Ocean from 60 degrees South to 54 degrees North, *J. Geophys. Res.*, *95*, 20,623–20,632.

Xie, P. P., and P. A. Arkin (1997), Global precipitation: A 17-year monthly analysis based on gauge observations, satellite estimates, and numerical model outputs, *Bull. Am. Meteorol. Soc.*, *78*, 2539–2558.